Reconstruction of a 2-D binary obstacle by controlled evolution of a level-set

A Litman†‡, D Lesselier† and F Santosa¶

† Laboratoire des Signaux et Systèmes, CNRS - Supélec, Plateau de Moulon, 91192 Gif-Sur-Yvette Cedex, France

‡ Now at the Faculty of Electrical Engineering, Eindhoven University of Technology, P.O. Box 513, 5600 MB Eindhoven, The Netherlands

¶ School of Mathematics, University of Minnesota, 127 Vincent Hall, 206 Church Street, Minneapolis MN 55455, USA

Abstract. We are concerned with the retrieval of the unknown cross-section of a homogeneous cylindrical obstacle embedded in a homogeneous medium and illuminated by time-harmonic electromagnetic line sources. The dielectric parameters of the obstacle and embedding materials are known and piecewise constant. That is, the shape (here, the contour) of the obstacle is sufficient for its full characterization. The inverse scattering problem is then to determine the contour from the knowledge of the scattered field measured for several locations of the sources and/or frequencies. An iterative process is implemented: given an initial contour, this contour is progressively evolved such as to minimize the residual in the data fit. This algorithm presents two main important points. The first one concerns the choice of the transformation enforced on the contour. We will show that this involves the design of a velocity field whose expression only requires the resolution of an adjoint problem at each step. The second one concerns the use of a level-set function in order to represent the obstacle. This level-set function will be of great use to handle in a natural way splitting or merging of obstacles along the iterative process. The evolution of this level-set is controlled by a Hamilton-Jacobi-type equation which will be solved by using an appropriate finite-difference scheme. Numerical results of inversion obtained from both noiseless and noisy synthetic data illustrate the behavior of the algorithm for a variety of obstacles.

Short title: Reconstruction of a 2-D binary obstacle by controlled evolution of a level-set

January 8, 1998

1. Introduction

In this paper, we investigate the solution of a nonlinear inverse scattering problem, i.e., the retrieval of the cross-section contour of a cylindrical homogeneous penetrable (lossy dielectric) obstacle located in free space (typically, air). The contrast of permittivity between the obstacle and its embedding is known, but main topological information is missing: the cross-section of the obstacle has no assumed connectivity (there may be an unknown number of isolated components), is not (or its components) necessarily star-shaped with respect to a given point, and no interior point is given. In effect the only such information is that the obstacle cross-section is contained in a given test domain, and that the contour has some degree of smoothness. Otherwise, measurements of the scattered field at several sensor locations around the obstacle and for several locations and/or frequencies of time-harmonic E-polarized line sources placed nearby are available. Such data will be synthetically generated by solving the associated direct problem with taking care not to commit the inverse crime, or obtained from independent investigators (Belkebir and Tijhuis 1996).

The two main questions in this so-called binary configuration - at any point of the test domain the permittivity contrast is either 0 (free space) or the prescribed value - is how to keep and take advantage of the binary aspect, and how to overcome the lack of topological information underlined above. The development as discussed next of a novel inversion algorithm based on the controlled (in some sense, optimal) evolution of a level set, will show that these two questions can be answered rather effectively.

Obviously, the 2-D scalar scattering case attacked here (a transmission problem in $\mathbb{R}^2$) remains somewhat canonical; however we believe that the analysis is still illustrative of the strengths and weaknesses of such an algorithm whereas extensions to more realistic environments, e.g., stratified ones for which only aspect-limited data are available (Lesselier and Duchêne 1996) and/or more realistic obstacles, e.g., 3-D bounded ones (Angell *et al* 1987), and consequently to more complicated scalar and vector wavefields, could be dealt with in a similar fashion. In particular, notice that some results are already available, though in a linearized framework, for the retrieval of cylindrical obstacles in a conductive half-space at eddy current frequencies (Litman *et al* 1997).

Several methods which take into account the binarity of the solutions have been developed through the literature. Some of them include this binarity by discretizing the test domain into white and black pixels and by letting these pixels evolve according to simulated annealing algorithms where the cost functional to minimize includes connectivity constraint so as to privilege the regrouping of either black or white pixels (see in a linearized framework, (de Oliveira Bohbot *et al* 1996)).

Others, which also aim at the retrieval of the test domain as a distribution of black

and white pixels, use the modified gradient technique (Kleinman and van den Berg 1992), with replacing the 0-1 contrast by a continuous approximation to a step function so as to restore the needed differentiability of the cost functional versus this contrast, and with reducing in an appropriate step-by-step fashion the discrepancy between the step function and its approximation so as to get a sharper and sharper map (Souriau *et al* 1996).

A large class of algorithms amounts to solving an equation which involves the contour of the unknown domain or its representative coefficients (Kirsch and Kress 1993) (Colton and Monk 1994) (Rozier *et al* 1997) (Angell *et al* 1997). In some representative cases it is assumed that the contour of the obstacle is obtained by a succession of small perturbations which are to minimize a normed discrepancy between the observed field (the data) and the theoretical field (the one associated to the iterated contour). For example, if Ω_t represents the domain of the scatterer at step t, the domain at the next iteration will be obtained through a certain deformation T, $\Omega_{t+1} = T(\Omega_t)$. To our knowledge so far, for problems of wavefield inversion, only one type of deformation has been examined closely. This deformation consists in a small perturbation of the identity and takes the following form: $T_h(\Omega_t) = \{y \in \mathbb{R}^n, y = x + h(x), \forall x \in \Omega_t\}$. (Masmoudi 1987) and (Kirsch 1993) both used this idea in order to solve the exterior Dirichlet problem. (Potthast 1996) considered the exterior Neumann problem. (Hettlich 1995) focussed on the exterior Robin problem as well as on the transmission problem. (Hettlich and Rundell 1996) applied these techniques to an inverse potential problem. (Roy *et al* 1997) investigated the inverse acoustic scattering problem of sound-hard obstacles.

The algorithm which is developed in this paper uses the same notion of shape deformation through an iterative process with ensuring that the chosen cost functional is decreased. However, this algorithm differs by two main choices from the previous ones: the type of deformation of the obstacle contour, and the type of representation of the obstacle cross-section, as follows.

First, instead of using the previous transformation, we implement a more general shape deformation (Céa 1976) (Sokolowski and Zolésio 1992) which is inspired from continuum mechanics (Germain 1973). This type of deformation, which is completely characterized by its velocity as discussed later, enables us to derive a closed form of the derivative of the cost functional with respect to a perturbation of the geometry. Furthermore, it may give us an idea of the asymptotical behavior of the solution when the number of iterations increases.

Second, the widely applied star-shaped representation of the boundary of the domain (Colton and Kress 1992) (Rozier *et al* 1997) (Kirsch 1993) is not adopted because it is not capable of retrieving multiple objects when the initial guess is a single one ((Haas *et al* 1997) reconstructed two objects, but from two initial ones). So, the key idea is to define the boundary of the object as the level 0 (a front) of a function of higher

dimension. Then, one can employ the level-set modeling technique (Osher and Sethian 1988) which easily handles the moving and possible splitting of the fronts. This is illustrated by various examples: crystal growth (Sethian and Strain 1992), and image processing (Malladi *et al* 1995) (Caselles *et al* 1993), while the feasibility of such an approach in the case of inverse problems involving obstacles such as the reconstruction of a diffraction screen has been shown recently (Santosa 1996).

The paper is organized as follows. In section 2 the problem of interest is introduced. In section 3 some general results on shape deformation are presented. In section 4 the cost functional (the error in the data fit), which is a shape functional, is shown to be Fréchet-differentiable with respect to the domain (the cross-section). This derivative involves the definition of an adjoint problem as well as the velocity of the deformation. This velocity is here to control the evolution such that the cost functional is decreased. In section 5 the level-set representation is introduced. This representation leads to a Hamilton-Jacobi-type equation which links the velocity to the level-set function. Through this equation, the deformation of the cross-sectional contour can be found. In section 6 the numerical implementation of the algorithm, inspired from a numerical scheme due to Osher and Sethian and borrowed from hyperbolic conservation laws, is described in detail. In section 7 numerical examples are introduced and discussed (no theoretical results of convergence of the whole scheme are available, and emphasis is then on the numerical experimentation). A short conclusion follows. In Appendix A complementary elements are introduced, in particular the material and shape derivatives of the field are exhibited. More details and results can be found in (Litman 1997).

2. Transmission problem

The model is the following : a z-oriented cylindrical obstacle, of cross-section Ω, is embedded in an homogeneous space $\Omega_E = \mathbb{R}^2 \setminus \bar{\Omega}$. The obstacle is assumed to be linear, isotropic, non-magnetic and penetrable and to have a sufficiently smooth boundary Γ. Its exterior normal is denoted by $\vec{n}$. The wave numbers $k_S(\omega)$, $k_E(\omega)$ ($\Im k_E(\omega)$, $\Im k_S(\omega) \geq 0$) of the different materials are assumed to be known for each frequency ω and to be independent of the position (the time dependance $\exp(-j\omega t)$ is chosen and dropped out from now on). An incident wave u^i of same cylindrical dependence (line source) illuminates the obstacle. We restrict ourselves to a Transverse Magnetic (TM) or E-polarization configuration. The total field u satisfies the following set of equations:

$$\Delta u + k_S^2 u = 0 \qquad \text{in } \Omega \tag{1a}$$

$$\Delta u + k_E^2 u = 0 \qquad \text{in } \Omega_E \tag{1b}$$

$$u^- = u^+ \qquad \text{on } \Gamma \tag{1c}$$

$$\frac{\partial u^+}{\partial \vec{n}} = \frac{\partial u^-}{\partial \vec{n}} \qquad \text{on } \Gamma \tag{1d}$$

where $u^+(u^-)$ denotes the limit of u from the exterior (interior) of Ω. The scattered field $u^s = u - u^i$ satisfies the Sommerfeld radiation condition

$$\lim_{r\to\infty} \sqrt{r}(\frac{\partial u^s}{\partial r} - jk_E u^s) = 0 \tag{2}$$

where $r = |x|$ and $j^2 = -1$. (Hettlich 1995), among others, has shown that this transmission problem has a unique solution $u \in H^1_{loc}(\mathbb{R}^2)$ for a given domain Ω.

The inverse problem consists in finding the shape Ω which minimizes the error on the data fit. If we denote by $L^2(M)$ the set of the measured scattered fields, where M is the probing line, the cost functional to minimize is of the following form:

$$J(\Omega) = \tfrac{1}{2} \parallel u^s(\Omega) - g \parallel^2_{L^2(M)} \tag{3}$$

where g corresponds to the data. The inverse problem can then be written as:

$$\text{Find } \Omega^* \text{ such that } J(\Omega^*) = \min_{\Omega} \tfrac{1}{2} \parallel u^s(\Omega) - g \parallel^2_{L^2(M)} \tag{4}$$

3. Shape deformation

Shape deformation has been introduced in order to solve shape optimization problems. In this case, the variable is no longer a function but the shape of a geometric domain Ω. Shape optimization thus consists in finding the geometry which minimizes a cost functional while satisfying a certain number of constraints. For example, how to draw a plane wing such that its air drag is minimal ? How to decrease the weight of a bicycle while keeping its robustness ? (Haug and Céa 1981) give an excellent overview of typical practical problems.

Usually, such problems are solved by using iterative schemes and in doing so by constructing a family of shapes Ω_t, $\Omega_0 = \Omega$, that are perturbations of Ω for $0 \leq t < \epsilon$ (Figure A1), t being a fictitious time parameter. These admissible domains Ω_t are assumed to be subsets of a larger fixed domain D and to keep the same regularity C^k.

The next question is how to define this family of perturbations. One could use the notions developed in continuum mechanics (Germain 1973) where a family of transformations $T_t : \bar{D} \to \mathbb{R}^2$ for $0 \leq t < \epsilon$ can be constructed such that :

$$x_t = T_t(x) \qquad \Omega_t = T_t(\Omega) \tag{5}$$

The perturbation of the identity

$$T_t(x) = x + t\theta(x) \tag{6}$$

where θ is of class C^k, is part of these transformations. (Murat and Simon 1976), among others, have introduced this diffeomorphism which (Kirsch 1993) (Hettlich 1995), for example, have used to solve inverse scattering problems.

One could also use a more general method denoted as the Velocity Method (Céa 1976) (Zolésio 1979). Instead of being defined by its transformation T_t, the deformation is defined by its velocity $\vec{V}(t,x) \in (C[0,\epsilon[, V^k(D))$ where $V^k(D)$ is the space of functions k-continuously differentiable with compact support included in D and such that these functions leave the boundary of D unchanged in order that the admissible domains Ω_t remain subsets of D, that is:

$$\vec{V} \cdot \vec{n} = 0 \text{ on } \partial D \text{ except on the points where the normal is undefined}$$
$$\vec{V}(x) = 0 \text{ for all singular points } x$$

In fact, these two definitions of the perturbation are equivalent. Indeed, for a given transformation T_t and under sufficient regularity condition, it is possible to associate a unique velocity field $\vec{V}(t,x)$, and vice-versa (Sokolowski and Zolésio 1992) (Delfour and Zolésio 1992). The velocity field is given by :

$$\vec{V}(t,x) = (\frac{\partial}{\partial t} T_t) \circ T_t^{-1}(x) \tag{7}$$

In short, a point is described by its initial position and the value of its velocity at time t.

To our knowledge, the deformation of the domain by a velocity field has not been widely used in the context of wavefield inversion. However, as we shall see, the formalism involved can be used to solve the inverse problem under consideration. Moreover, it also enables to choose the deformation more freely and to have an idea of the evolution of the scheme when t is large. Finally, let us emphasize that this kind of transformation provides us with expressions of the derivatives that are easy to compute.

As the cost functional depends on a variable which is not a function anymore, the usual definitions of derivatives are evidently to be adapted. Following Cea's works (Céa 1976), Zolésio has used notions already found in continuum mechanics (Germain 1973), such as the material derivative, while introducing a complementary notion of shape derivative (see the comprehensive exposé of (Sokolowski and Zolésio 1992)). Such an analysis is now developed.

4. Fréchet-derivative of the cost functional

We are interested in obtaining a closed form of the derivative of the cost functional according to a perturbation of the geometry. In order to do so, we could either look at the weak formulation of the Helmholtz equations (1), or apply integral equations methods. When considering the perturbation of the identity (6), (Kirsch 1993) (Hettlich 1995) have used the first formulation while (Potthast 1996) (Charalambopoulos 1995) have considered the second one.

Following Hettlich's notations, we choose to introduce a weak formulation of the transmission problem. A ball B_R with radius $R > 0$ such that $\bar{\Omega} \subseteq B_R$ is chosen.

The Dirichlet-to-Neumann map L is defined in order to incorporate the Sommerfeld radiation condition:

$$\begin{aligned} L : H^{1/2}(\partial B_R) &\to H^{-1/2}(\partial B_R) \\ f &\to \frac{\partial w}{\partial \vec{n}} \end{aligned}$$

where w is the unique solution of the exterior Dirichlet problem in $\mathbb{R}^2 \setminus \bar{B}_R$ with boundary data $w = f$. The total field $u = u(\Omega) \in H^1(B_R)$ satisfies the following variational equation:

$$\mathcal{S}(u, v) = \int_{B_R} (\nabla u \nabla \bar{v} - \kappa^2 u \bar{v}) \, \mathrm{d}x - < Lu, v > \; = (f, v)_{H^1(B_R)} \tag{8}$$

for all $v \in H^1(B_R)$ where

$$\kappa^2(x) = \begin{cases} k_S^2 & \text{for } x \in \Omega \\ k_E^2 & \text{for } x \in \Omega_E \end{cases} \tag{9}$$

$< \cdot, \cdot >$ represents the scalar product in the duality $H^{-1/2}(\partial B_R), H^{1/2}(\partial B_R)$ and $\mathcal{S}$ a sesquilinear form : $H^1(B_R) \times H^1(B_R) \to \mathbb{C}$. The function $f \in H^1(B_R)$ represents the linear functional

$$\int_{\partial B_R} (\frac{\partial u^i}{\partial \vec{n}} - Lu^i) \, \bar{v} \, \mathrm{d}s = (f, v)_{H^1(B_R)} \tag{10}$$

In the transmission problem, the space definition of the fields does not change along the iterations, i.e., $u \in H^1(B_R)$ instead of $u \in H^1(\Omega)$. This is of great help when differentiating with respect to the domain. When defining the velocity, we introduced a hold-all domain D, which can be considered here as B_R. In order to avoid a problem at the boundary, the velocity $\vec{V}$ is assumed to have a compact support strictly included in B_R. The boundary of B_R is then totally invariant. We also assume that the probing line M is not a part of the support of $\vec{V}$.

The first step consists in differentiating the total field $u(\Omega)$ with respect to Ω and thus obtaining its shape derivative.

4.1. Material and shape derivative

In order to obtain the shape derivative of the total field, we need to prove that its material derivative exists. The material derivative $\dot{u}(\Omega, \vec{V})$ of $u(\Omega)$ for a given velocity $\vec{V} \in C([0, \epsilon[, V^k(B_R))$ is defined by:

$$\dot{u}(\Omega, \vec{V}) = \lim_{t \to 0} \frac{1}{t} \left(u(\Omega_t) \circ T_t - u(\Omega) \right) \tag{11}$$

Then, if the domains Ω_t are sufficiently smooth, the following proposition holds.

Proposition Let $\vec{V} \in C([0, \epsilon[, V^k(B_R))$ a velocity field with compact support strictly included in B_R, then the solution u of the transmission problem has a strong material

derivative $\dot{u} \in H^1(B_R)$ in the direction $\vec{V}$. This material derivative is the unique solution of the following variational equation for all $v \in H^1(B_R)$:

$$\mathcal{S}(\dot{u}, v) = \int_{B_R} < A'(0) \cdot \nabla u, \nabla v > - \kappa^2 \gamma'(0)\ u(x)\ \bar{v}(x)\ \mathrm{d}x \tag{12}$$

where γ' denotes the derivative of $\gamma(t) = det(DT_t)$, DT_t being the Jacobian matrix of the transformation T_t and where A' denotes the derivative of $A(t) = \gamma(t)(DT_t)^{-1}(*DT_t)^{-1}$.

In order to define the shape derivative, we also need that the quantity $\nabla u \cdot \vec{V}(0)$ belongs to $H^1(B_R)$. This comes from the fact that the normal components of the fields are continuous on the boundary of Ω_t ($u \in H^2(B_R)$). The following proposition can then be stated.

Proposition Let $\vec{V} \in C([0, \epsilon[, V^k(B_R))$ a velocity field with compact support strictly included in B_R, then the solution u of the transmission problem has a shape derivative $u' \in H^1(B_R)$ in the direction $\vec{V}$. This shape derivative is the unique solution of the following variational equation for all $v \in H^1(B_R)$:

$$\mathcal{S}(u', v) = -\int_\Gamma \left[\nabla u(\nabla v^+ - \nabla v^-) + u(k_E^2 \bar{v}^- - k_S^2 \bar{v}^+)\right]\ \vec{V}(0) \cdot \vec{n}\ \mathrm{d}\sigma \tag{13}$$

Both proofs are given in Appendix A.

4.2. Derivative of the cost functional

The cost functional is of the following form:

$$J(\Omega) = \tfrac{1}{2}\ \|\ u^s(\Omega) - g\ \|^2_{L^2(M)} \tag{14}$$

As the incident field is independent of the shape, the scattered field has the same shape derivative as the total field. Furthermore, the probing line M is fixed, so the Eulerian derivative of the cost functional in the direction $\vec{V}$ is of the following form:

$$dJ(\Omega, \vec{V}) = \Re \int_M u'(y)\overline{(u^s - g)}(y)\mathrm{d}y \tag{15}$$

In order to simplify this expression, we introduce an adjoint state p defined by:

$$\Delta p + k_S^2 p = -\overline{(u^s - g)}\ \delta_M \qquad \text{in } \Omega \tag{16a}$$

$$\Delta p + k_E^2 p = 0 \qquad \text{in } \Omega_E \tag{16b}$$

$$p^- = p^+ \qquad \text{on } \Gamma \tag{16c}$$

$$\frac{\partial p^+}{\partial \vec{n}} = \frac{\partial p^-}{\partial \vec{n}} \qquad \text{on } \Gamma \tag{16d}$$

where δ_M denotes the Kronecker symbol. This adjoint state is solution of the following variational equation:

$$\mathcal{S}(p, \psi) = \int_\Gamma \overline{(u^s - g)}(y)\ \bar{\psi}(y)\ \mathrm{d}y \qquad \forall \psi \in H^1(B_R) \tag{17}$$

Replacing ψ by $\bar{u}'$ in (17) and v by $\bar{p}$ in (8), since u and p belong to $H^2(B_R)$ the combination of the two equations leads to:

$$\int_M u'(y)\overline{(u^s - g)}(y)\mathrm{d}y = \int_\Gamma (k_S^2 - k_E^2)\; u(\sigma)p(\sigma)\; \vec{V}(0)\cdot\vec{n}\;\mathrm{d}\sigma \tag{18}$$

The Eulerian derivative of the cost functional can then be expressed by:

$$dJ(\Omega, \vec{V}) = \Re \int_\Gamma (k_S^2 - k_E^2)\; u(\sigma)p(\sigma)\; \vec{V}(0)\cdot\vec{n}\;\mathrm{d}\sigma \tag{19}$$

5. Shape representation

In order to implement numerically this iterative process, a suitable representation of the binary object is needed. The level-set representation is the second key-point of this work. It enables to overcome a large number of topological difficulties.

5.1. Level-set representation

There are several possible representations which can retain the binary aspect of the scattering object through the iterative process. One could think about pixels, for example (de Oliveira Bohbot *et al* 1996): "black" pixels will represent the object, and "white" pixels the surrounding. The main difficulty is to let these pixels evolve in a continuous fashion.

One could follow some points on the boundary of the domain Ω_t. For example, (Zolésio 1979) (Masmoudi 1987) (Vincent *et al* 1997) use Finite Element Methods for solving the direct problem which lead them to let the mesh grid evolve through the iterations. For the scattering problem, one can use the Method of Moments which, with the changing boundary, would also be computationally prohibitive as one needs to calculate a new set of Green's function with each iteration.

One could also associate a parametrization to the boundary of the domain, for example, a star-shaped representation (Rozier *et al* 1997) (Colton and Kress 1992). This representation can easily describe the contour but it has several drawbacks. This representation is non-intrinsic, i.e., several representations can give rather different results. Star-shaped objects depends on the origin point, which has to be inside the object: this implies the advance knowledge of the number of objects and accordingly one or several appropriate interior points. Furthermore, merging or splitting of objects has to be handled with care and requires a supplementary algorithmical effort.

Recently (Santosa 1996) proposed to represent the contour through a function of higher dimension. If the star-shaped representation can be viewed as a Lagrangian representation, the level-set one is similar to an Eulerian representation. Santosa introduces a level-set ϕ, $\phi \in C^1(B_R)$ with $\| \nabla\phi \|$ such that (figure A2):

$$\Gamma_t = \{x \in B_R \;\mid\; \phi(t,x) = 0\} \tag{20}$$

$$\Omega_t = \{x \in B_R \mid \phi(t,x) < 0\} \tag{21}$$

With this representation, there is no need of a priori knowledge on the number of objects, on their origin and so on. The definition of the contour is implicit and made in a geometrical fashion. Furthermore, splitting and merging can be handled in a natural way.

5.2. Hamilton-Jacobi equation

The evolution of the level-set will directly lead to the evolution of the domain. The main question now is to characterize this evolution. If we differentiate one level contour, say, contour $\phi = C$ according to t, we get (Santosa 1996):

$$\frac{\partial}{\partial t}\phi(t,x) + \vec{V}(t,x)\cdot\vec{n}\,|\nabla\phi(t,x)| = 0 \tag{22}$$

as $\frac{\partial}{\partial t}x = \vec{V}(t,x)$ and $\vec{n} = \nabla\phi/|\nabla\phi|$. This equation (22) is a Hamilton-Jacobi type equation, where the velocity $\vec{V}$, which is still to be chosen within the previously discussed framework, plays an important role.

This type of equation is frequently found in image processing, for example in edge detection process. A geometrical approach of deformable models for edge detection has been proposed independently by (Caselles *et al* 1993) and (Malladi *et al* 1995). In both models, the motion of the surface is controlled by a Hamilton-Jacobi equation. (Malladi *et al* 1995)'s work is based on a previous study of (Osher and Sethian 1988) on the problem of flame propagation. By representing the front of the flame with a level-set function, they end up with the same kind of equation. They have introduced a finite-difference upwind numerical scheme borrowed from conservation laws. The main advantage of this scheme, apart from being stable and entropy satisfying, is that one can use a fixed cartesian grid through the iterative process. This scheme will be employed here.

5.3. Velocity choice

The velocity is controlling the evolution of the scheme and an appropriate choice is thus essential.

Since the Fréchet-derivative of the cost function (19) and the Hamilton-Jacobi equation (22) only require the normal component of the velocity, we restrict ourselves to velocities which have the same direction as the normal:

$$\vec{V}(t,x) = V(t,x)\,\vec{n}(t,x) \tag{23}$$

We then have to choose the amplitude. This amplitude must be such that the domain Ω_t tends to the "exact" domain when $t \to \infty$. Several proposals are available (Zolésio

1979) (Céa 1976) (Malladi *et al* 1995). The choice taken here is more an empirical one and enables to define the velocity on the whole test domain (this is required by the finite-difference scheme which solves the Hamilton-Jacobi equation (22)):

$$V(t,x) = -(k_S^2 - k_E^2)\, u_t(x)\, p_t(x) \qquad \forall x \in B_R \tag{24}$$

The velocity is taken as minus what is left under the integral in the Fréchet derivative of the cost function (19). This should lead us to a cost function which decreases at each step.

6. Numerical process

In this section, we will give some useful hints for the numerical implementation of such algorithm.

6.1. Initialisation

The first step in this iterative process is to define an initial shape of the object. This can be done either by choosing the domain Ω_0 and deducing the level-set $\phi(0,x)$ or vice-versa. The first option is taken here. The initial domain is only constrained by the fact that at least one pixel of the domain must belong to Ω_0 in order to compute the associated level-set.

The choice of the initial domain can otherwise be arbitrary. It can be made of one or several components, connected or not. It can also be deduced from a previous treatment of the data through a backpropagation scheme (Kleinman and van den Berg 1992).

Once the initial shape Ω_0 is given, a level-set function in the test domain must be associated to its contour. The choice of this level-set is also quite free. Following Osher and Sethian, we define the level-set as the oriented distance function:

$$\phi(0,x) = \begin{cases} -\mathrm{dist}(x, \partial\Omega_0) & \text{if } x \in \Omega_0 \\ +\mathrm{dist}(x, \partial\Omega_0) & \text{if } x \notin \Omega_0 \end{cases} \tag{25}$$

6.2. Fields calculations

At each step, we have to compute a direct field u_t and an adjoint field p_t. In fact, both problems can be reduced to a single one. The only difference comes from the source terms on the right hand-side of the Helmholtz equations (1) (16). For the adjoint problem, the sources are in fact set at the receiver locations, and their amplitude depends on the difference between the scattered field u_t^s and the measured field g. In order to reduce the computation cost, we are using a domain integral representation of the fields as well as a Method of Moments in order to solve the equations numerically. The choice of the MoM requires the computation of two Green's matrices, one which corresponds to the

interaction between a point in the test domain and a point on the probing line, the other to the interaction between two points of the test domain. These matrices do not depend on the incident field and if the discretisation mesh is fixed, they do not change through the iterations. Since the numerical scheme which enables to follow the evolution of the domain Ω_t keeps the grid fixed, we then need to compute these matrices only once. This represents a large saving in the computational time and would not have been possible if we where using boundary integral representations. Indeed, at each step, we would have to detect the points of the boundary $\partial\Omega_t$ and to recompute the Green's matrices at these points.

6.3. Numerical Hamiltonian

Once the velocity is chosen, all coefficients which are involved in the Hamilton-Jacobi equation are defined. It remains to deform the level-set. This implies to compute what is called a numerical Hamiltonian. The Hamilton-Jacobi equation is replaced by:

$$\frac{1}{\Delta t}\left(\phi_{ij}^{t+1} - \phi_{ij}^{t}\right) - V_{ij}^{t}\, H(\phi_{ij}^{t}) = 0 \tag{26}$$

where w_{ij}^t denotes the value taken by the function w at the point (x_i, y_j) at time t and where H corresponds to the numerical Hamiltonian which is in fact an approximation of the gradient $|\nabla\phi|$. The main difficulty is how to define the numerical Hamiltonian. The scheme is described in detail in (Osher and Sethian 1988) (Sethian 1990). In the following, we will just make some remarks.

The first one concerns the sign of the velocity. Indeed, this sign greatly influences the scheme if it is not properly taken into account. The choice made here is such that the domain should expand when the velocity is positive. This leads to:

- if $V_{ij}^t \geq 0$, the numerical Hamiltonian is given by:
  $H(\phi_{ij}^t)^2 = \max(D_-^x \phi_{ij}^t, 0)^2 + \min(D_+^x \phi_{ij}^t, 0)^2 + \max(D_-^y \phi_{ij}^t, 0)^2 + \min(D_+^y \phi_{ij}^t, 0)^2$
- if $V_{ij}^t < 0$, then:
  $H(\phi_{ij}^t)^2 = \min(D_-^x \phi_{ij}^t, 0)^2 + \max(D_+^x \phi_{ij}^t, 0)^2 + \min(D_-^y \phi_{ij}^t, 0)^2 + \max(D_+^y \phi_{ij}^t, 0)^2$

where $D_+^x \phi_{ij}^t = (\phi_{i+1,j}^t - \phi_{i,j}^t)/\Delta x$ and $D_-^y \phi_{ij}^t = (\phi_{i,j}^t - \phi_{i,j-1}^t)/\Delta y$.

The second remark concerns the boundary conditions to impose on the level-set. Since the velocity has been taken such that the boundary of the test domain should remain fixed, the level-set function verifies a Neumann boundary condition. This condition is implemented numerically.

The last remark concerns the time step Δt. The space step Δx and Δy are conditionned by the MoM. The time step depends on the Courant-Friedrich-Leroy condition that the numerical scheme of Osher and Sethian must satisfy. We will see in the following section the influence of this parameter on the convergence of the algorithm.

6.4. Algorithm

Let us briefly summarize the algorithm:

- Initialisation process:
  - Choose the initial domain Ω_0 either arbitrarily or by backpropagation.
  - Define the level-set obtained through the oriented distance function (25).
  - Compute the total field u_0 and the scattered field u_0^s.
- As long as $J(\Omega_t) > Tol$, where Tol is a given error:
  - Compute the adjoint field p_t (16).
  - Compute the velocity V_{ij}^t (24).
  - Deform the level-set function ϕ (26).
  - Get the level-set 0 to obtain Ω_{t+1}.
  - Compute the total field u_t and the scattered field u_t^s as well as the new cost function $J(\Omega_{t+1})$.

7. Numerical results

Here are presented illustrative results of the inversion (more results are available in (Litman 1997)). The first set of reconstructions concerns one single obstacle. This set is meant to get an idea of the influence of the different parameters on the reconstruction process. The second set deals with the reconstruction of several obstacles, starting from a single initial one.

7.1. One obstacle

7.1.1. Configuration The homogeneous background in which is situated the obstacle is air ($\epsilon_E = \epsilon_0$,$\sigma_E = 0$, μ_0). The area in which the obstacle can be found is a square test domain of length side $d = \lambda$, and centered at $(0, 0)$. Only one frequency is used, 10 GHz ($\lambda = 3$ cm). The receivers and the sources are equally spaced on a circle of radius $\lambda/2$ and centered at $(0, 0)$. The number of receivers is equal to the number of sources, i.e., 10.

The test domain is divided into square cells. The number of cells varies between the direct problem (43×43) and the inverse one (21×21) in order to prevent ourselves of an inverse crime. In both cases, the size of the cells is sufficiently small according to the MoM criteria.

The obstacle under study is a disk of radius $\lambda/4$, centered at $(\lambda/6, -\lambda/6)$ as shown in figure A3. Its dielectric characteristics ($\epsilon_S = 1.8\epsilon_0$, $\sigma_S = 0$, μ_0) are known. The contrast of permittivity thus takes the value $\chi = 0.8$ inside the obstacle and 0 outside.

7.1.2. Evolution process Let us first illustrate the evolution of the different functions along the iterative process. The initial guess is a disk of radius $\lambda/4$, centered at $(0,0)$ (Figure A4). The time step is $\Delta t = 10^{-2}$. No noise has been added. This configuration will be taken as the basis in the following comparisons. The algorithm stops according to two criteria: either the normalized error (the difference between the measured and computed scattered fields divided by the norm of the measured scattered fields) gets lower than a certain tolerance number (here 10^{-2}), either the number of iterations reaches a certain step (here 300).

In figure A5, one follows the evolution of the retreived contour towards the "exact" contour. In figure A6, one follows the deformation of the level-set function. The minimum of the level-set function actually tends to move itself where the "exact" solution is. Even more significant is the evolution of the velocity (Figure A7). After the first iteration, the velocity is negative where the initial guess is situated, i.e., this velocity is asking to "remove" some points there, and is positive where the "exact" obstacle is supposed to be. Furthermore, through the iterations, the amplitude of the velocity decreases and tends to a plateau. This is one of the signs of the convergence of the algorithm.

7.1.3. Time step The time step has a strong influence on the convergence of the scheme. In figure A8, one can see how the normalized error behaves when we change this time step. The rapidity of the convergence increases when increasing the time step until a certain tolerance value is reached beyond which the process diverges.

7.1.4. Noisy data White Gaussian noise has been added to the scattered fields. For different values of the signal-to-noise ratio, the normalized error is plotted (Figure A9). After a certain number of steps, no more information is added. The deformations left are only done on the noisy part of the data and correspond for the reconstructed domain to the appearance/disappearance of one or two pixels.

7.1.5. Initial guess As previously said, the initial domain can be chosen almost arbitrarily. Several choices are illustrated in figure A10: a large disk of radius $\lambda/2$ and centered at $(0,0)$, an isolated pixel centered at $(0,0)$ and the backpropagated solution. The latter has been truncated according to its average value in order to get a binary estimate. In all cases, the final reconstruction is similar and very close to the "exact" obstacle. The influence of such a choice is then very small in such configuration.

7.1.6. Contrast error So far, we have assumed that the values of the dielectric characteristics were known. What happens if the given values are not the correct ones can be seen in figure A11. In the first case, the contrast is divided by a factor

2 ($\epsilon_S = 1.4\epsilon_0$). The final image is well-positionned but occupies twice much more space than the "exact" one. In the second case, the contrast is multiplied by 2 ($\epsilon_S = 2.6\epsilon_0$). The result is not very good.

7.2. Several obstacles

The obstacles under study are contained into a square domain test of 2 m by side. There are made of two disks and one ring. The disks of radius 0.2 m are centered at $(0.3, 0.6)$ m and $(-0.3, 0.6)$ m. The ring has an exterior radius of 0.6 m and an inner radius of 0.3 m, and is centered at $(0, 0.2)$ m. This configuration is also refered as the "Austria" profile (Belkebir and Tijhuis 1996). The background is made of air and the contrast between the obstacles and the surrounding is of value 1. 64 sources and 64 receivers are equally placed on a circle of radius 3 m centered at $(0, 0)$.

The simulated data that we are using for the reconstruction has been provided by Belkebir and Tijhuis. They use the MoM associated with CGFFT procedures (Peng and Tijhuis 1993) in order to compute the scattered field and a discretisation of 65×65 cells. Those fields are given at several frequencies : 100, 200, 300 and 400 MHz.

Tijhuis and Belkebir input these data in their own inversion algorithm. Their technique of "marching-on-in frequency" is as follows: for each frequency, the data are treated separately, from the lowest to the highest frequency. The initial guess corresponds to the result of the last iteration of the previous treated frequency.

The same approach has been followed here. The parameters are the following ones. The test domain is discretised into 30×30 cells, the time step is 0.05 and the error tolerance is 0.01. Several initial guesses have been considered. The main problem in this "Austria" profile is the hole in the ring. A backpropagated solution did not give satisfactory results. The best result is obtained when one chooses a centered disk of radius 1 m, i.e., half the dimension of the test domain. In figure A12, one can see the final results obtained at each frequency. The lower frequency gives an overall view of the obstacle. Higher frequencies increase the resolution of the reconstruction. One can also notice that we are able to reconstruct several obstacles starting from a single one, without any a priori information on their number or positions.

8. Conclusion

We have developed here a novel iterative algorithm for solving the nonlinear wavefield inversion problems in the particular case of the so-called binary medium, where the contrast function at any point of the search domain is allowed to take only one of two prescribed values. The novelty of this algorithm is due to the alliance of (i) a representation of the surface enclosing domains of same contrast (the level-set representation), which only requires rather weak topological constraints, and (ii) a mode

of evolution of the surface as a function of a fictitious time (the Velocity Method), which only requires to calculate the shape derivative of the cost functional, which can be obtained through a standard adjoint problem.

In current practice, and in addition to the choice of an appropriate time step (by numerical experimentation so far) the success of the approach relies on the choice of the velocity field, since this field directly controls the evolution of the level set function and consequently the decrease of the cost functional. However the choice made here is one of the simplest ones available, and indeed yields a very good reconstruction of the obstacles, but the choice may turn out to be more critical when, for example, the embedding configuration is more complicated (see the illustrative case of a stratified configuration (Litman *et al* 1997)). At the theoretical level, there is a need to understand the regularity of the Velocity Method when the level-set undergoes a topological change during iterations. Numerical results appear to support the notion that while the velocity field may become singular, the level-set function remains regular.

We emphasize that the method is not restricted to a 2-D geometry, E-polarized scalar fields, with full viewing of the obstacle. For more complicated environments, and more restricted datasets, the critical point may be the choice of velocity, as indicated before. Difficulties may also arise when writing down the adjoint problem if different boundary conditions are to be considered. Enforcing supplementary constraints on the level set, say, by looking for obstacles of minimum extent or for surfaces of least curvature, is also a subject clearly open to further investigation. As for the computational burden it should increase quite a lot with the consideration of vector fields, Green's dyads and 3-D obstacles (depicted as a level-set function of dimension 4), since one is solving one direct problem and one adjoint problem at each time step, but then every other algorithm faces the same prognosis. Finally, notice that we have restricted ourselves to the reconstruction of binary obstacles, but it would be interesting to see whether the method could be applied to obstacles whose contrast is now allowed to take several prescribed values, or even more to slowly varying domains limited by sharp boundaries.

Acknowledgments

The support of a CNRS-NSF International Cooperation Grant ♯ INT - 9415493 is acknowledged. A Litman also benefited from a grant from the Institute for Mathematics and its Applications, Minneapolis, MN, which allowed her to visit Minnesota in order to collaborate with F Santosa on this project. The authors gratefully acknowledge helpful discussion with J P Zolésio on the Velocity Method, and theoretical issues surrounding it. They would also like to thank A G Tijhuis and K Belkebir for providing the data of the "Austria" profile. The research of F Santosa is partially supported by NSF under grant DMS-9503114, DoE under grant DE-FG02-94-ER25225, and AFOSR under grant

F49620-95-1-0305.

Appendix A. Material and shape derivative of the total field

The total field $u = u(\Omega)$ is solution of the transmission problem (1). It equivalently satisfies the variational equation (8) where $\mathcal{S}$ is sesquilinear form. (Hettlich 1995) has shown that $\mathcal{S}(u,v) = (S(u),v)_{H^1(B_R)} = (f,v)_{H^1(B_R)}$ and that the operator $S : H^1(B_R) \to H^1(B_R)$ is inversible and its inverse is bounded.

A family of perturbations Ω_t of Ω is constructed. At each Ω_t is associated a field $u_t = u(\Omega_t)$, solution of the perturbed transmission problem, which satisfies the following perturbed variational equation:

$$\mathcal{S}_t(u_t,v_t) = \int_{B_R} (\nabla u_t \nabla \bar{v}_t - \kappa_t^2 u_t \bar{v}_t)\,\mathrm{d}x - < Lu_t, v_t > \; = (f,v_t)_{H^1(B_R)} \tag{A1}$$

for all $v_t \in H^1(B_R)$ where

$$\kappa_t^2(x) = \begin{cases} k_S^2 & \text{for } x \in \Omega_t \\ k_E^2 & \text{for } x \in \mathbb{R}^2 \setminus \bar{\Omega}_t \end{cases} \tag{A2}$$

With (Sokolowski and Zolésio 1992) notations, for example, $g^t = g_t \circ T_t(\vec{V})$, the change of variables in the previous integral equation gives:

$$\mathcal{S}_t(u^t,v^t) = \int_{B_R} < A(t)\nabla u^t, \nabla v^t > -\kappa^2 u^t v^t \gamma(t)\mathrm{d}x - < Lu^t, v^t > = (f^t,v^t)_{H^1(B_R)} \tag{A3}$$

This comes from the fact that the velocity $\vec{V}$ has been chosen in order to let the boundary of B_R invariant along the iterations. Thus, $g^t \mid_{\partial B_R} = g_t \mid_{\partial B_R}$. This holds as well for Lu^t or f^t and v^t on the boundary of the ball B_R. Since the right-hand-side of (8) and (A3) are equivalent, we finally get $\mathcal{S}(u,v^t) = \mathcal{S}_t(u^t,v^t)$ for all $v^t \in H^1(B_R)$.

From the definitions of the sesquilinear forms we obtain for all $\phi, \psi \in H^1(B_R)$, $\mathcal{I}$ being the identity operator:

$$\mathcal{S}_t(\phi,\psi) - \mathcal{S}(\phi,\psi) \;\; = \int_{B_R} < (A(t)-\mathcal{I})\cdot\nabla\phi, \nabla\psi >_{\mathbb{C}^2} -\kappa^2(\gamma(t)-1)\phi\bar{\psi}\,\mathrm{d}x \tag{A4}$$

$$\begin{aligned} |\mathcal{S}(\phi,\psi) - \mathcal{S}_t(\phi,\psi)| \leq & \left(\int_{B_R} \nabla\phi\nabla\bar{\psi} + \phi\bar{\psi}\,\mathrm{d}x\right) \\ & \times \left(\parallel A(t) - \mathcal{I} \parallel_{L^\infty(B_R,\mathbb{R}^{2^2})} + \parallel \gamma(t) - 1 \parallel_{L^\infty(B_R)} \parallel \kappa^2 \parallel_{L^\infty(B_R)}\right) \end{aligned} \tag{A5}$$

Since

$$\frac{1}{t}(A(t)-\mathcal{I}) \to A'(0) \qquad \text{strongly in } L^\infty(B_R,\mathbb{R}^{2^2}) \tag{A6}$$

$$\frac{1}{t}(\gamma(t)-1) \;\to \gamma'(0) \qquad \text{strongly in } L^\infty(B_R) \tag{A7}$$

we can deduce that S is continuous according to t. Using a perturbation argument (Colton and Kress 1992) (Kress and Zinn 1992), we can conclude the continuous dependence $u_t \to u \in H^1(B_R)$.

Appendix A.1. Material derivative

We will now focus on the material derivative $\dot{u}$ of u. Let $z^t = \frac{1}{t}(u^t - u) \in H^1(B_R)$, we get:

$$\begin{aligned}\mathcal{S}(z^t - \dot{u}, v) &= \tfrac{1}{t}\mathcal{S}(u^t - u, v) - \mathcal{S}(\dot{u}, v) \\ &= \int_{B_R} < \frac{1}{t}(A(t) - \mathcal{I}) \cdot \nabla u^t - A'(0) \cdot \nabla u, \nabla v > \, \mathrm{d}x \\ &\quad - \int_{B_R} \kappa^2 \left[\frac{1}{t}(\gamma(t) - 1)u^t - \gamma'(0)u\right] \bar{v} \, \mathrm{d}x\end{aligned}$$

As $u^t \to u$ in $H^1(B_R)$, its gradient ∇u^t converges strongly to ∇u in $L^2(B_R,\mathbb{C}^2)$. Thus:

$$\tfrac{1}{t}(A(t) - \mathcal{I}) \cdot \nabla u^t - A'(0) \cdot \nabla u \to 0 \qquad \text{strongly in } L^2(B_R,\mathbb{C}^2) \tag{A8}$$

$$\tfrac{1}{t}(\gamma(t) - 1)\, u^t - \gamma'(0)\, u \qquad \to 0 \qquad \text{strongly in } L^2(B_R) \tag{A9}$$

It follows:

$$|\mathcal{S}(z^t - \dot{u}, v)| \leq \epsilon(t) \parallel v \parallel_{H^1(B_R)} \qquad \forall v \in H^1(B_R) \tag{A10}$$

where $\epsilon(t) \to 0$ when $t \to 0$. Taking $v = \mathcal{S}(z^t - \dot{u})$ in the previous inequality leads to a majoration in $\epsilon(t)$ of $\parallel \mathcal{S}(z^t - \dot{u}) \parallel_{H^1(B_R)}$. As S is inversible and its inverse is bounded, we can deduce that z^t converges strongly towards $\dot{u} \in H^1(B_R)$.

Thus, the material derivative $\dot{u}$ in the direction $\vec{V} \in C([0, \epsilon[, V^k(B_R))$ satisfies the following variational equation:

$$\mathcal{S}(\dot{u}, v) = \int_{B_R} < A'(0) \cdot \nabla u, \nabla v > - \kappa^2 \gamma'(0)\, u(x)\bar{v}(x) \, \mathrm{d}x \tag{A11}$$

Appendix A.2. Shape derivative

The shape derivative is defined if the material derivative exists, as we have just shown, and if the quantity $\nabla u \cdot \vec{V}(0)$ belongs to $H^1(B_R)$. This comes from the continuity of the normal components on the boundary of Ω.

In order to define this shape derivative u', we differentiate the variational equation (A3) that u_t satisfies. This can be simply done when using the following result:

$$\frac{\mathrm{d}}{\mathrm{d}\Omega} \int_\Omega u(\Omega)\mathrm{d}x = \int_\Omega u'(\Omega, \vec{V})\mathrm{d}x + \int_\Gamma u(\Omega)\, \vec{V}(0) \cdot \vec{n}\mathrm{d}\sigma \tag{A12}$$

The shape derivative is then solution of the following variational equation:

$$\mathcal{S}(u', v) = -\int_\Gamma \left[\nabla u(\nabla v^+ - \nabla v^-) + u(k_E^2 \bar{v}^- - k_S^2 \bar{v}^+)\right] \, \vec{V}(0) \cdot \vec{n} \, \mathrm{d}\sigma \tag{A13}$$

References

Angell T S, Jiang X and Kleinman R E 1997 A distributed source method for inverse acoustic scattering *Inverse Problems* **13** 531–546

Angell T S, Kleinman R E and F R G 1987 An inverse transmission problem for the Helmholtz equation *Inverse Problems* **3** 149–180

Belkebir K and Tijhuis A G 1996 Using multiple frequency information in the iterative solution of a two-dimensional nonlinear inverse problem *Proc. PIERS 96: Progress in Electromagnetics Research Symposium (Innsbruck, Austria)* p 353

Caselles V, Catté F, Coll T and Dibos F 1993 A geometric model for active contours in image processing *Numer. Math.* **66** 1–31

Céa J 1976 Une méthode numérique pour la recherche d'un domaine optimal *Publication IMAN* (Université de Nice)

Charalambopoulos A 1995 On the Fréchet-differentiability of boundary integral operators in the inverse elastic scattering problem *Inverse Problems* **11** 1137–1162

Colton D and Kress R 1992 *Inverse Acoustic and Electromagnetic Scattering Theory* (Berlin: Springer-Verlag)

Colton D and Monk P 1994 The detection and monitoring of leukemia using electromagnetic waves: mathematical modelling *Inverse Problems* **10** 1235–1252

de Oliveira Bohbot O, Lesselier D and Duchêne B 1996 Mapping defects in a conductive half-space by simulated annealing with connectivity and size as constraints *J. Electromagn. Waves Applic.* **10** 983–1004

Delfour M C and Zolésio J P 1992 Structure of shape derivatives for nonsmooth domains *J. Func. Anal.* **104** 1–33

Germain P 1973 *Cours de Mécanique des Milieux Continus* (Paris: Masson)

Haas M, Rieger W, Rucker W and Lehner G 1997 Inverse 2D electromagnetic obstacle scattering for multiple scatterers using an iterative adaptation technique *Proc. IEEE Antennas and Propagation Soc. Int. Symp. 1997 (Montreal, Canada)* pp 1722–1725

Haug E J and Céa J 1981 *Optimization of Distributed Parameter Structures* (The Netherlands: Sijthoff and Noordhoff)

Hettlich F 1995 Fréchet derivatives in inverse obstacle scattering *Inverse Problems* **11** 371–382

Hettlich F and Rundell W 1996 Iterative methods of the reconstruction of an inverse potential problem *Inverse Problems* **12** 251–266

Kirsch A 1993 The domain derivative and two applications in inverse scattering theory *Inverse Problems* **9** 81–96

Kirsch A and Kress R 1993 Uniqueness in inverse obstacle scattering *Inverse Problems* **9** 285–299

Kleinman R E and van den Berg P M 1992 A modified gradient method for two-dimensional problems in tomography *J. Comput. Appl. Math.* **42** 17–35

Kress R and Zinn A 1992 On the numerical solution of the three-dimensional inverse obstacle scattering problem *J. Comput. Appl. Math.* **42** 49–61

Lesselier D and Duchêne B 1996 Wavefield inversion of objects in stratified environments. From backpropagation schemes to full solution *Review of Radio Science 1993-1996* ed R Stone *et al* (Oxford: Oxford University Press) pp 235–268

Litman A 1997 Deux méthodes d'inversion pour la caractérisation électromagnétique ou acoustique d'objets enfouis: transformée de Fourier-Laplace inverse et déformation d'ensembles de niveaux

Thèse de Doctorat en Sciences (Université Paris XI Orsay)

Litman A, Lesselier D and Santosa F 1997 A level-set approach for eddy current imaging of defects in a conductive half-space *Inverse Problems of Wave Propagation and Diffraction* ed Chavent G and Sabatier P C (Berlin: Springer Verlag) pp 250–262

Malladi R, Sethian J A and Vemuri B C 1995 Shape modelling with front propagation: a level set approach *IEEE Trans. Pattern Anal. Machine Intel.* **17** 158–175

Masmoudi M 1987 Outils pour la conception optimale de formes *Thèse d'Etat en Sciences Mathématiques* (Université de Nice)

Murat F and Simon J 1976 Sur le contrôle par un domaine géométrique *Publications du Laboratoire d'Analyse Numérique* (Université Paris VI)

Osher S and Sethian J A 1988 Fronts propagating with curvature-dependent speed: algorithms based on Hamilton-Jacobi formulations *J. Comput. Phys* **79** 12–49

Peng Z Q and Tijhuis A G 1993 Transient scattering by a lossy dielectric cylinder: marching-on-in-frequency approach *J. Electromagn. Waves Applic.* **7** 739–763

Potthast R 1996 Fréchet differentiability of the solution to the acoustic neumann scattering problem with respect to the domain *J. Inverse Ill-Posed Probl.* **4** 67–84

Ghosh Roy D N, Couchman L and Warner J 1997 Scattering and inverse scattering of sound-hard obstacles via shape deformation *Inverse Problems* **13** 585–606

Rozier C, Lesselier D, Angell T and Kleinman R E 1997 Shape retrieval of an obstacle immersed in shallow water from single frequency fields using a complete family method *Inverse Problems* **13** 487–508

Santosa F 1996 A level-set approach for inverse problems involving obstacles *ESAIM: COCV* **1** 17–33

Sethian J A 1990 Numerical algorithms for propagating interfaces: Hamilton-Jacobi equations and conservation laws *J. Differential Geometry* **31** 131–161

Sethian J A and Strain J 1992 Crystal growth and dendritic solidification *J. Comput. Phys.* **98** 231–253

Sokolowski J and Zolésio J P 1992 *Introduction to Shape Optimization. Shape Sensitivity Analysis* (Heidelberg: Springer Verlag)

Souriau L, Duchêne B, Lesselier D and Kleinman R E 1996 A modified gradient approach to inverse scattering for binary objects in stratified media *Inverse Problems* **12** 463–481

Vincent P, Saillard M and Bonnard S 1997 Cross-borehole inverse scattering using a conjugate gradient algorithm *Proc. PIERS 97: Progress in Electromagnetics Research Symposium (Boston, USA)* p 553

Zolésio J P 1979 Identification de domaines par déformations *Thèse d'Etat en Mathématiques* (Université de Nice)

Figure captions

Figure A1 : Domain perturbations of Ω: $\Omega_t = T_t(\Omega)$

Figure A2 : Level-set function

Figure A3: "Exact" single obstacle

Figure A4: Initial estimate of the domain

Figure A5: Evolution of the domain through the iterations

Figure A6: Evolution of the level-set function through the iterations

Figure A7: Evolution of the velocity through the iterations

Figure A8: Error according to time step Δt,
$(+)$ $\Delta t = 10^{-3}$, $(——)$ $\Delta t = 10^{-2}$, $(*)$ $\Delta t = 510^{-2}$

Figure A9: Error according to signal-to-noise ratio,
$(——)$ No noise, $(+)$ S/N = 20 dB, $(*)$ S/N = 10 dB, $(\triangle)$ S/N = 5 dB

Figure A10: Reconstructions for different initial guesses

Figure A11: Final reconstructions for different inexact values of the permittivity

Figure A12: Reconstruction of the "Austria" profile

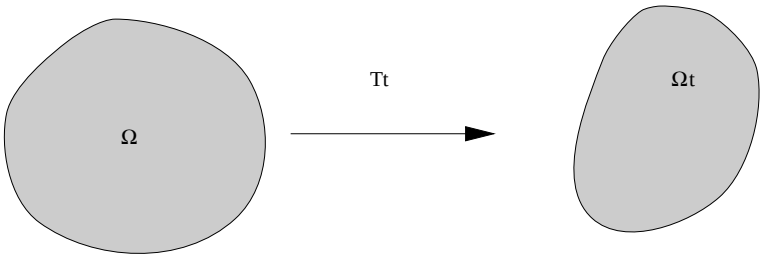

Figure A1. Domain perturbations of Ω: $\Omega_t = T_t(\Omega)$

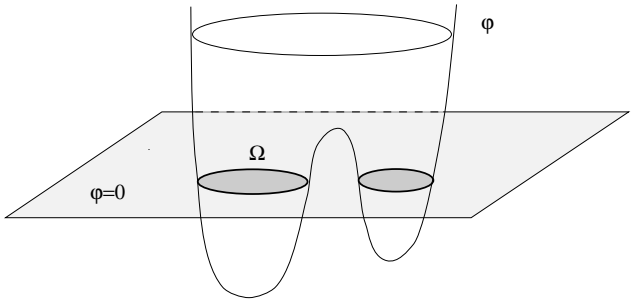

Figure A2. Level-set function

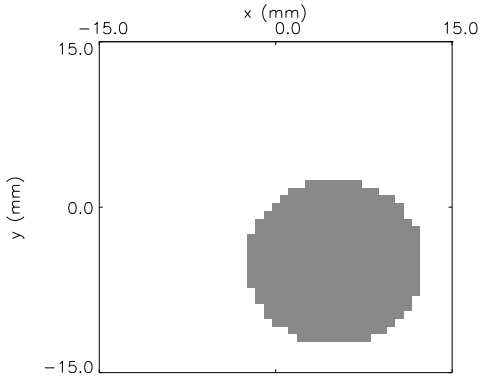

Figure A3. "Exact" single obstacle

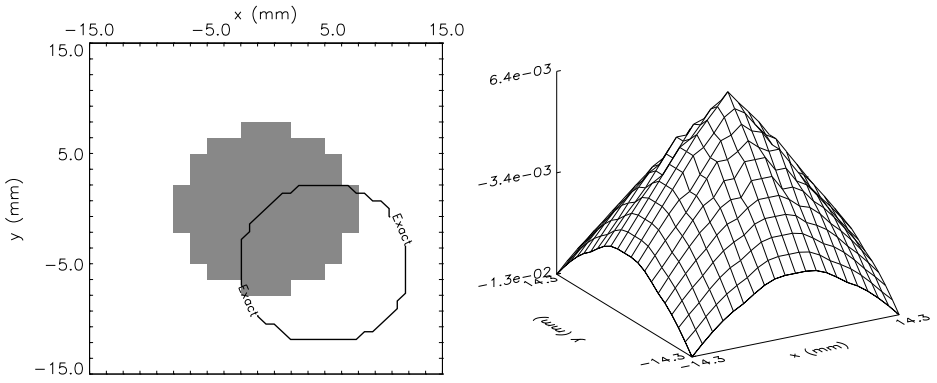

(a) Domain Ω_0 (b) Level-set $-\phi(0,x)$

Figure A4. Initial estimate of the domain

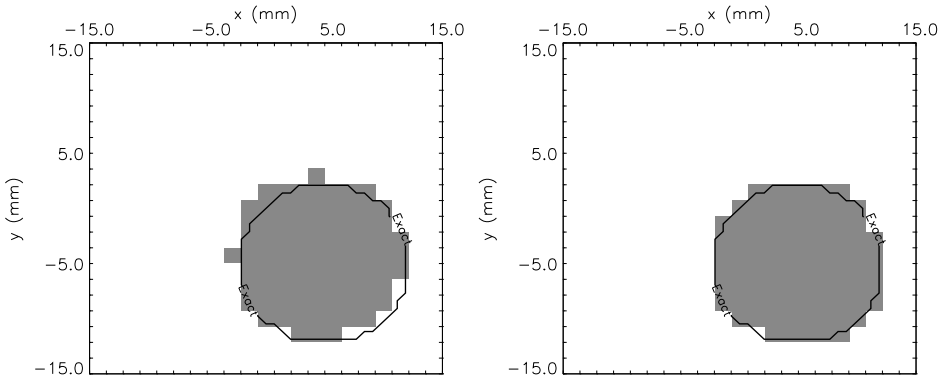

(a) iteration 20 (b) iteration 39

Figure A5. Evolution of the domain through the iterations

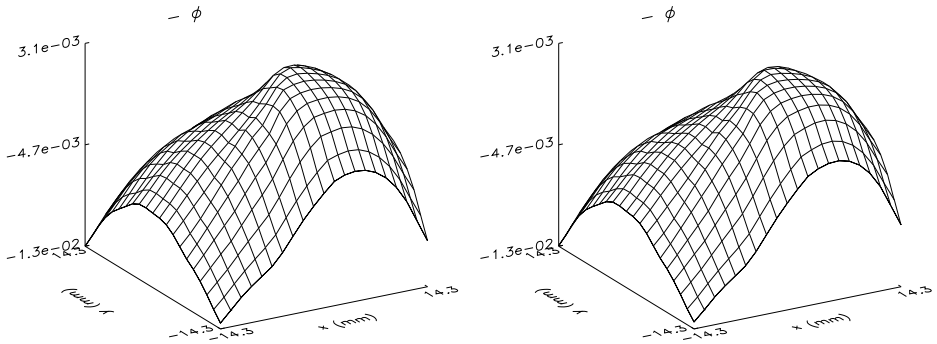

(a) $-\phi$ at iteration 20 (b) $-\phi$ at iteration 39

Figure A6. Evolution of the level-set function through the iterations

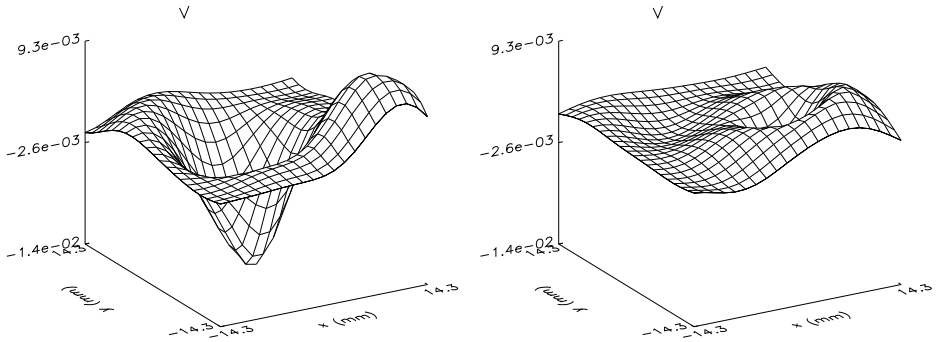

(a) V at iteration 20 (b) V at iteration 39

Figure A7. Evolution of the velocity through the iterations

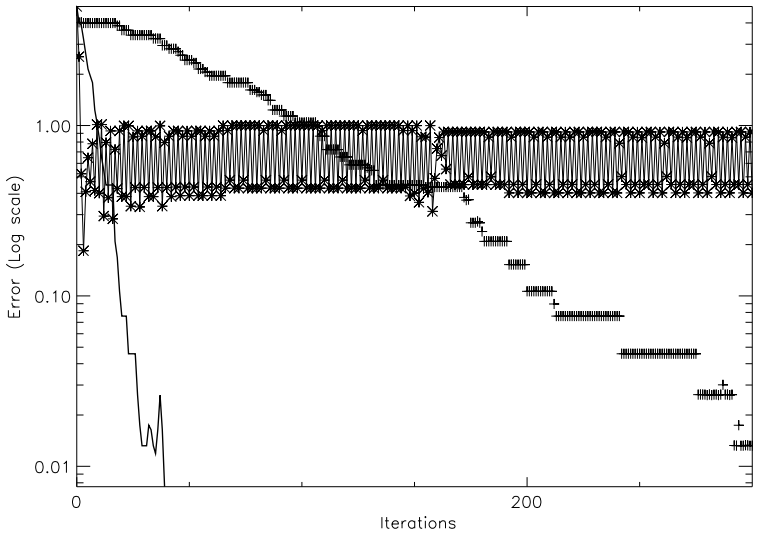

Figure A8. Error according to time step Δt
(+) $\Delta t = 10^{-3}$, (——) $\Delta t = 10^{-2}$, (∗) $\Delta t = 510^{-2}$

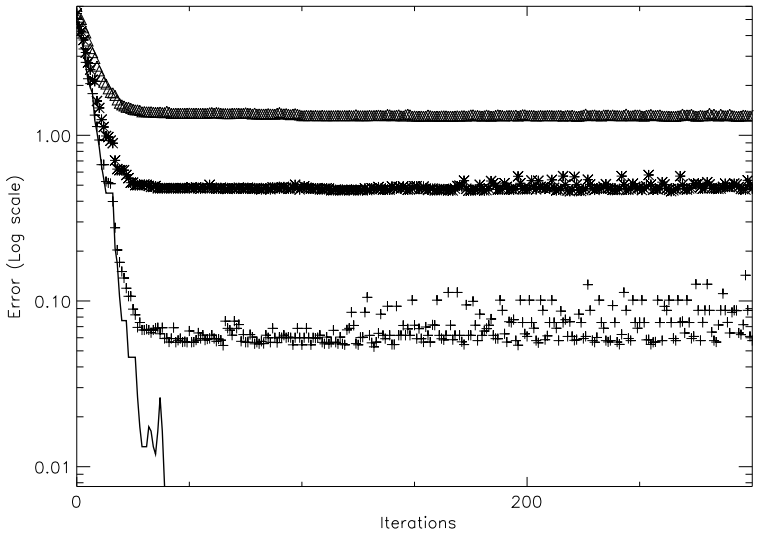

Figure A9. Error according to signal-to-noise ratio
(——) No noise, (+) S/N = 20 dB, (∗) S/N = 10 dB, (△) S/N = 5 dB

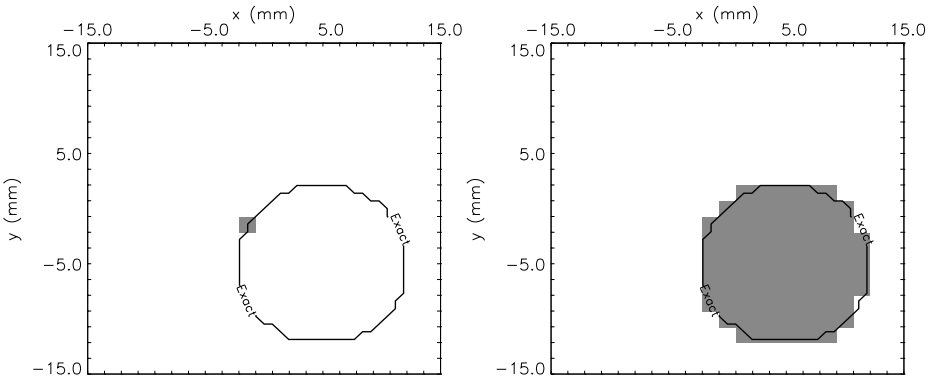

(a) Only 1 pixel as an initial guess and 27 iterations later

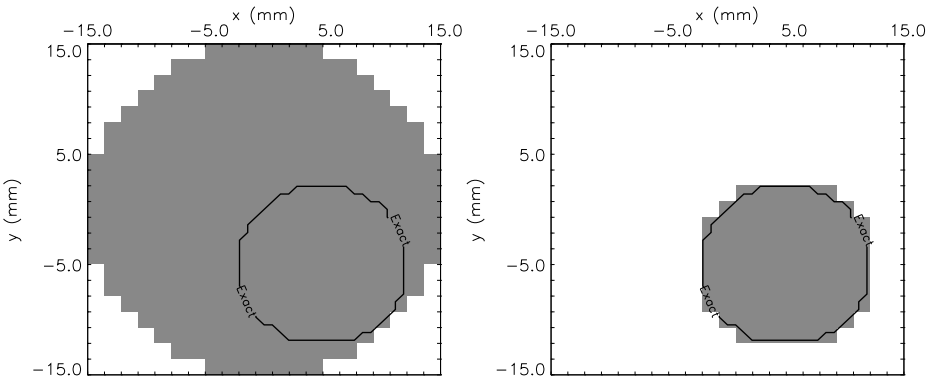

(b) Big circle as an initial guess and 39 iterations later

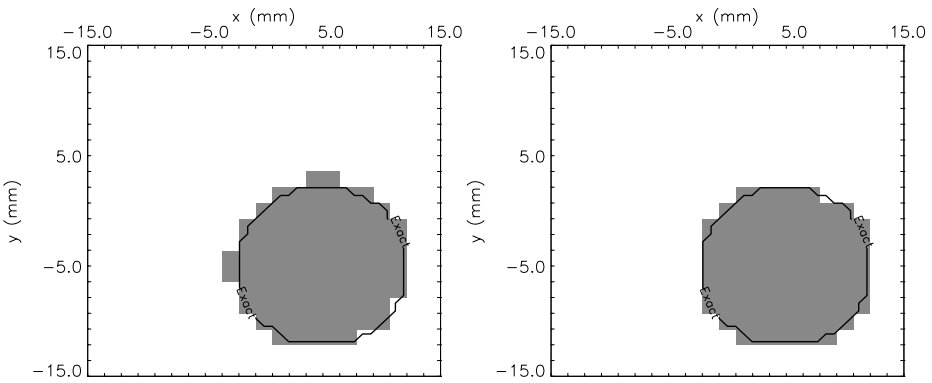

(c) Backpropagation as an initial guess and 20 iterations later

Figure A10. Reconstructions for different initial guesses

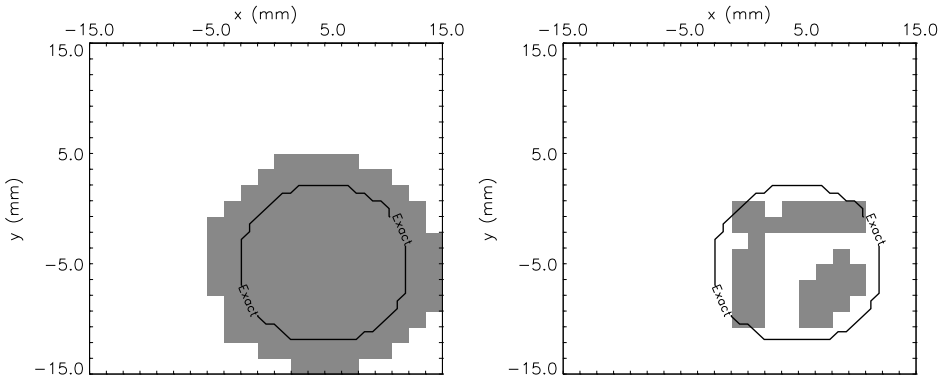

(a) $\varepsilon_S = 1.4\,\varepsilon_0$ at iteration 300 (b) $\varepsilon_S = 2.6\,\varepsilon_0$ at iteration 300

Figure A11. Final reconstructions for different inexact values of the permittivity

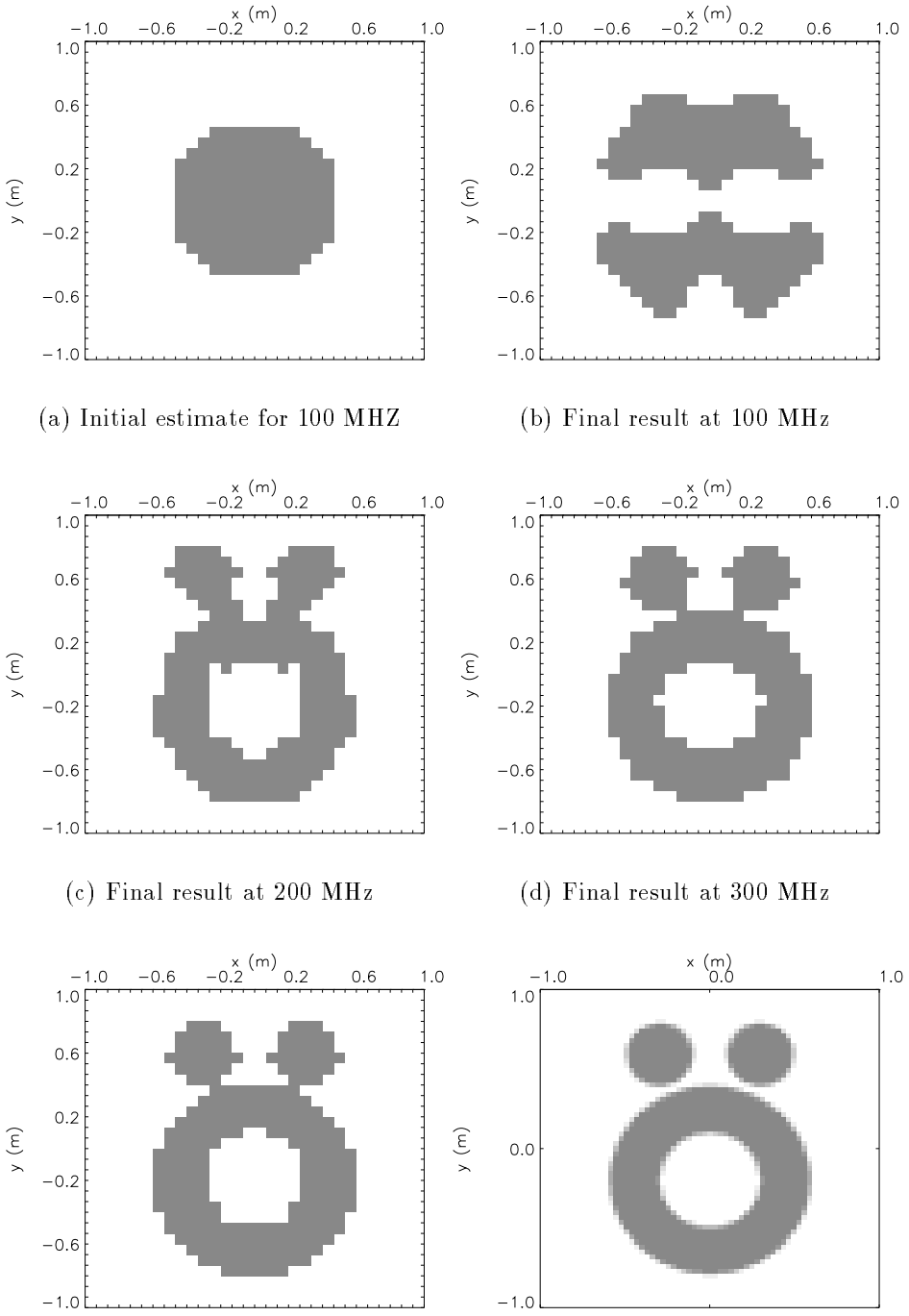

(a) Initial estimate for 100 MHZ

(b) Final result at 100 MHz

(c) Final result at 200 MHz

(d) Final result at 300 MHz

(e) Final result at 400 MHz

(f) Exact "Austria" profile

Figure A12. Reconstruction of the "Austria" profile